An equivalent isotropic approximation for reliability-based design of mini-plate fixation used in fractured mandibles

Une approximation isotrope équivalente pour la conception basée sur la fiabilité de la fixation par mini-plaques utilisées dans les mandibules fracturées

G. Kharmanda[1,2], M-Y Kharma[3], A. El-Hami[2]

[1] Department of Biomedical Engineering, Lund University / LTH, Lund, Sweden, ghias.kharmanda@bme.lth.se
[2] Mechanics Laboratory of Normandy, INSA Rouen, St Etienne du Rouvray, France, abdelkhalak.elhami@insa-rouen.fr
[3] Al-Farabi College for Dentistry, Jeddah, Saudi Arabia, mykharma@hotmail.com

RÉSUMÉ. L'objectif de ce travail est d'évaluer le niveau de fiabilité de la fixation par min-plaques suivante l'opération chirurgicale. Un modèle éléments finis en 3D est développé pour étudier les effets négatifs concernant la stabilité de la fracture. Durant l'opération chirurgicale, les muscles peuvent être abimées où coupées. Pour cela, l'incertitude sur le chargement doit être intégrée pour obtenir une conception fiable. Plusieurs scenarios (modes) peuvent conduire à la défaillance. Le scenario le plus important est les contraintes de von-Mises qui peuvent être comme indicateur de la fracture. L'os possède un comportement anisotrope. Pour cela, une approximation isotrope équivalente est intégrée pour réduire le temps de calcul. Le deuxième scenario est la pression de contact entre les surfaces de la fracture. Le troisième mode est le déplacement relatif maximal dans la zone de la fracture. An algorithme de fiabilité est développé pour identifier les différents modes de défaillance. Les résultats sont effectués sur une photo orthopantomogramme d'un patient male de l'âge de 28 ans.

ABSTRACT. The objective of this work is to assess the reliability level of mini-plate fixation following surgical operation. A 3-dimensional finite element model is developed in order to study the negative effect due to the stabilization of the fracture. Since muscles can be cut or harmed during surgery and consequentially cannot operate at its maximum capacity, there is a strong need to introduce loading uncertainties in order to obtain reliable designs. Several scenarios (or modes) may lead to failure. The first important failure scenario is the von Mises stress of all components which presents the fracture indicators. The bone structure possesses anisotropic behaviors. An optimized yield stress/elasticity modulus formulation is integrated using an equivalent isotropic approximation in order to reduce the computing time. The second failure scenario is the contact pressure which should not exceed a maximum pressure pain threshold. The last failure mode is the relative displacement (gap) between two fracture surfaces which should not exceed a prescribed value in order to obtain rapid bone healing. A reliability algorithm is next developed to identify the single and multiple failure mode cases. The different results are carried out considering a clinical case of a male patient of 28 years of age.

MOTS-CLÉS. Propriétés des matériaux osseux, Fractures de la mandibule, Fixation par mini-plaque, Optimisation des structures, Fiabilité structurale.

KEYWORDS. Bone Material Properties, Mandible Fractures, Mini-plate Fixation, Structural Optimization, Structural Reliability.

1. Introduction

Fracture of the mandible is one of the most common bone injuries, and the most common causes of injury are vehicle crashes, falls, violence, and sports. In a previous investigation related to mandible fracture [1], muscle forces were ignored, and the mandible is clamped at its ends. The only load was the bite force. For this loading case, Korkmaz [1] investigated several mini-plate systems and provided recommendations regarding mini-plate location, orientation, and type selection. Recently, several muscle forces are considered (masseter, temporalis, lateral and medial pterygoïd forces) in order to show the importance of these forces [2,3]. Among the data that need to be introduced inside numerical

models, material properties are of major importance [4]. The bone tissue is composed of inorganic and organic phases and water. On a weight basis, bone is approximately 60 percent inorganic, 30 percent organic, and 10 percent water [5,9]. Inorganic components are essentially responsible for the compression strength and stiffness, while organic components provide the corresponding tension properties. Recently, an optimized formulation developed by Kharmanda [10] was mainly based on the inorganic component effects (explicit relationship). According to several experimental works, some coefficients were added to the proposed model in order to take in account the organic component effects (implicit relationship). The mechanical properties of bone depend on its composition. However, composition is not constant in living tissues. It changes permanently in terms of the mechanical environment, ageing, disease, nutrition and other factors [11]. In this study, bone anisotropy should be introduced to take into account the directional variation of tissue properties and their evolution after mini-plate fixation as a function of the applied load magnitude. A direct simulation using bone anisotropy can be easily performed, however when considering reliability and optimization processes, several stress constraints (all directions) must be used. That leads to a very high computing time. To solve this problem, an equivalent isotropic approximation is integrated into an accurate optimized yield stress/elasticity modulus bone formulation.

Traditional deterministic design methods have accounted for uncertainties through empirical safety factors. The designer does not take into account uncertainties concerning materials, geometry and loading. A number of uncertainties are encountered during the design of replacement systems. These uncertainties are resulted from the variability of applied loads and materials properties, in addition to that resulting from the design modeling. They can be grouped in three main categories, namely irreducible, reducible and statistical uncertainties [12]. In the best scenario in the design of structural systems, uncertainties can be reduced or minimized but they cannot be completely eliminated. Thus, all parameters of interest in an engineering design can be considered as random variables [13]. In the present study, the different external forces are considered as uncertain parameters in the period following the surgical operation (convalescence period). In this case, it is considered that there can be a frictional contact between fracture surfaces. A reliability algorithm is next developed in order to assess the reliability level for single and multiple failure modes. An application on a clinical case of a male patient of 28 years of age is finally carried out to show the applicability of the proposed reliability strategy.

2. Methodologies and models

2.1. Problem description (clinical case study)

Fig. 1 presents an orthopantomogram of a male patient at the age of 28 years. The surgical operation was carried out at Aleppo University Hospital [14]. The current study is carried out after the operation in order to test its reliability level. There were no specific complications related to his treatment and the healing period was around 3 months. In the studied model, due to the limited influence of the teeth on the mechanical response of the mandible, these are ignored and removed in order to simplify the computational model. The mono-cortical screws were modeled as simple cylinders of length appropriate for penetration. The geometrical modeling of the composite structure is carried out using SolidWorks, however the numerical simulation and optimization procedures are performed using ANSYS software and APDL commands (ANSYS Parametric Design Language).

Fig. 1. *Orthopantomogram of a male patient of age 28 years [14].*

2.2. *Material properties: An equivalent isotropic approximation*

For the used material modeling, two elastic behaviors are considered: isotropic and orthotropic. The metallic parts (mini-plates and screws) are assumed to be elastic-isotropic and made of titanium with Young's modulus 110GPa, Poisson ratio 0.35, and yield stress 830MPa [15]. The mandible bone tissues are modeled using cancellous and cortical layers with elastic-orthotropic behavior [16,17]. Nine independent constants have to be used in the orthotropic case to reproduce the material symmetry with respect to two perpendicular planes. The values of these nine constants (Table 1) were taken from Castano et al. [18]. According to the optimized elasticity's modulus - yield stress (σ-E) bone formulation proposed by Kharmanda [10], the yield stress formulation for the cortical and cancellous bone can be written as follows:

$$\sigma_T = R_{T/C}.A_\sigma \left(\frac{E}{A_E}\right)^{R_{\sigma/E}}$$

(1)

where $A_E = 11142$, $A_\sigma = 129.5$ are optimized proportionality constants and $R_{\sigma/E} = 0.94$ is an optimized ratio (for details, see [10]). Different values have been used for the tension/compression ratio $R_{T/C}$, from 0.5 to 0.7 for cortical bone and from 0.7 to 1 for cancellous bone [11]. During habitual activities such as gait, the most produced stresses on femur and tibia bone are uniaxial that can be treated as isotropic materials [19]. However, in the mandible simulation, the directional variation of tissue properties are taken into account. The orthotropic material properties of the cortical and cancellous bone layers are considered. In order to apply Equation 1, an approximation based on strain energies equality proposed by Bonnet et al. [15] is used to determine Young's modulus E and Poisson's ratio ν of an equivalent isotropic medium. Here, the bulk modulus of the equivalent isotropic material is given as follows:

$$K = \frac{E_x E_y E_z}{(1-2\nu_{xz})E_y E_z + (1-2\nu_{yx})E_x E_z + (1-2\nu_{zy})E_x E_y}$$

(2)

and the shear modulus is given by:

$$G = \frac{3G_{xy}G_{yz}G_{zx}}{G_{yz}G_{zx} + G_{xy}G_{zx} + G_{xy}G_{yz}}$$

(3)

The equivalent Young's modulus can be written as

$$E = \frac{9KG}{3K+G}$$

(4)

and the equivalent Poisson's ratio as follows:

$$\nu = \frac{3K - 2G}{2(3K + G)} \tag{5}$$

The values of elastic constants obtained for cortical (symphyseal and rami areas) and cancellous bones are reported in Table 1 and the corresponding the yield stresses in compression and tension are evaluated using the optimized σ-E bone formulation.

2.3. Boundary conditions

In this study, several muscle forces are included in order to obtain realistic simulation models. During the bite process, the digastric muscles are not very active and therefore not included in analysis [3]. In Fig. 2, an illustration of the twelve muscle forces (six on each side) applied to the mandible are shown. The components of the applied forces are given in Table 2.
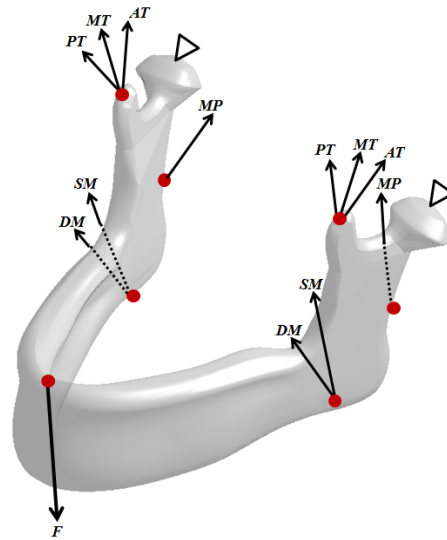

Fig. 2. Boundary conditions.

2.4. Reliability analysis

In structural reliability theory many effective techniques have been developed to estimate the reliability, namely FORM (First Order Reliability Methods), SORM (Second Order Reliability Method) and simulation techniques [12]. The transformation of the random variables $\mathbf{y}$ in the standard normalized space is denoted $\mathbf{u}$, calculated by: $\mathbf{u} = T(\mathbf{y})$ where $T(\mathbf{y})$ is the probabilistic transformation function. The mean value m_i of the random variable y_i corresponds to the origin in the normalized space (Fig. 2). The reliability assessment can be performed for a single failure mode and for multiple failure modes.

2.4.1. Single Failure Mode (S.F.M.)

For a given failure scenario $H(\mathbf{u}) = 0$, the reliability index β is evaluated by solving a constrained minimization problem:

$$\beta = \min \ d(\mathbf{u}) \quad \text{subject to:} \quad H(\mathbf{u}) = 0 \tag{6}$$

with

$$d = \sqrt{\sum u_i^2} \tag{7}$$

where $\mathbf{u}$ is the variable vector in the normalized space, measured from the origin see Fig. 3b.
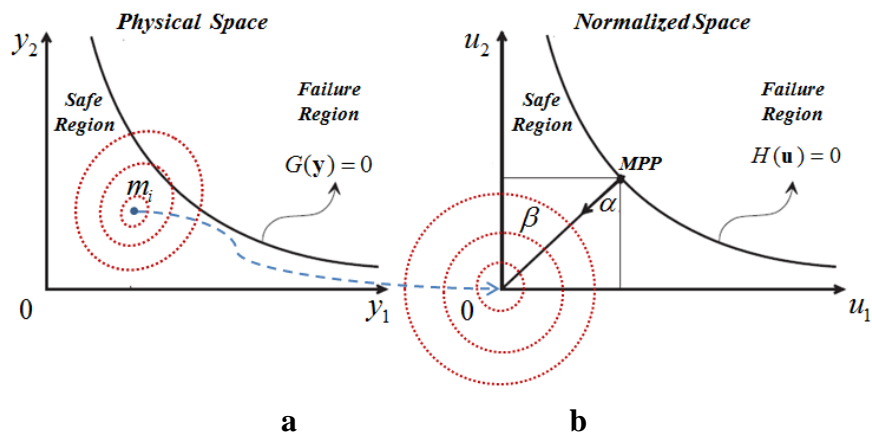
Fig. 3. *Physical and normalized spaces for single failure mode.*

The solution to problem (6) defines the **Most Probable failure Point (MPP)**, see Fig. 3b. The resulting minimum distance between the limit state function $H(\mathbf{u})$ and the origin, is called the reliability index β [20]. The reliability index that corresponds to the probability of failure, is numerically computed as follows

$$P_f \approx \Phi(-\beta_t) \tag{8}$$

where $\Phi(.)$ is the standard Gaussian cumulated function given as follows:

$$\Phi(Z) = \frac{1}{\sqrt{2\pi}} \int_{-\infty}^{Z} e^{-\frac{z^2}{2}} \, dz, \tag{9}$$

For practical structural engineering studies, Eq. (8) gives sufficiently accurate estimation of the failure probability [21]. Fig. 4 shows a flowchart of the MPP algorithm. It consists of two nested optimization loops: The objective of the first one is to find a failure point belonging to the limit state ($G(\mathbf{y}) = 0$) in the physical space, cf. Fig. 3a. The second loop tests the reliability levels for several failure points in order to find the MPP which belongs to the limit state ($H(\mathbf{u}) = 0$) in the normalized space. The MPP state is found at the minimum distance to the origin of the normalized space.
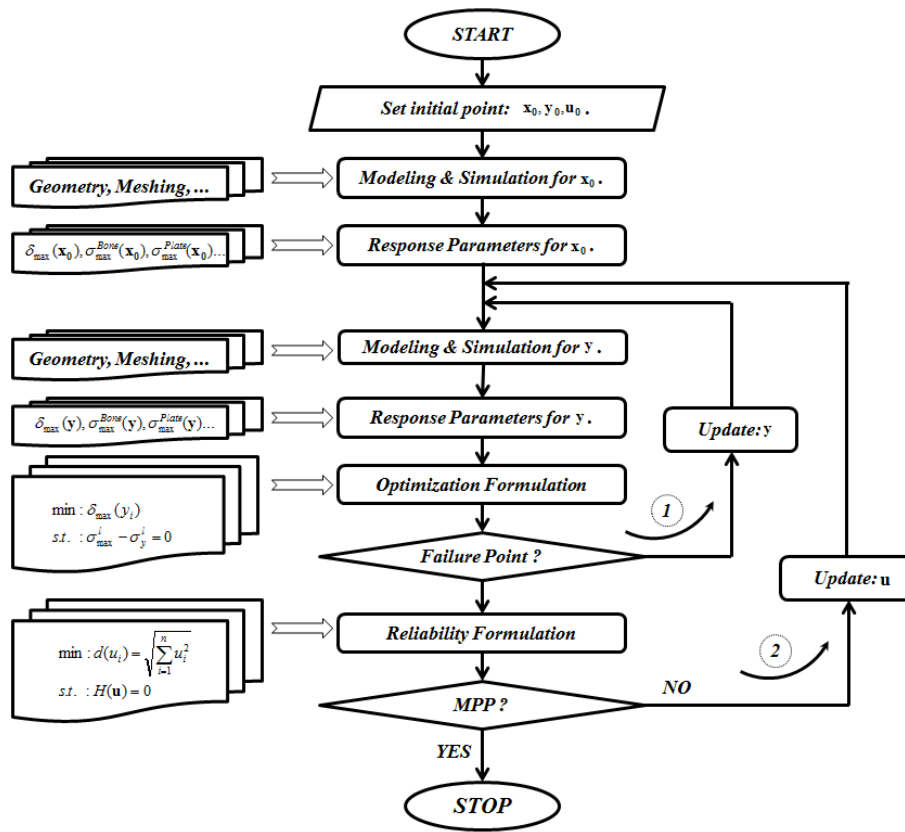
Fig. 4. *Flowchart of MPP algorithm.*

2.3.2. *Multiple Failure Modes (M.F.M.)*

When multiple conflicting criteria are involved and several constraint functions have to be used. The reliability index for multiple failure modes β_m can be evaluated by solving a constrained minimization problem:

$$\beta_m = \min \ d(\mathbf{u}) \quad \text{subject to:} \quad \mathbf{H}(\mathbf{u}) = \mathbf{0} \tag{10}$$

where $\mathbf{H}(\mathbf{u}) = \mathbf{0}$ is the vector of limit state functions (equality constraints). Fig. 5 shows a general illustrative example of the physical and the normalized spaces for double failure modes (limit states). The global optimum solution for double failure modes in the normalized space is presented by the minimum distance between the intersection point P^* and the origin. The developed reliability algorithm shown in Fig. 4 provides a global optimum within a reasonable computing time. In some special cases, the MPP can be coincided on the intersection point P^* (Fig. 5b).
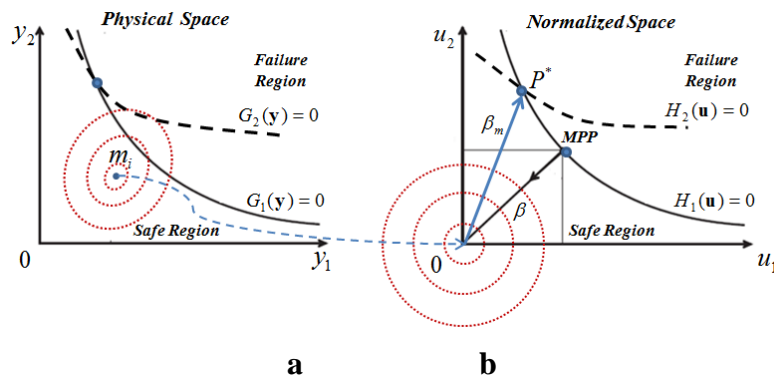

a   **b**

Fig. 5. *Physical and normalized spaces for multiple failure modes.*

3. Results

3.1. *Problem simulation*

The finite element simulation is carried out using ANSYS software. Fig. 6a shows a meshing model of cortical (symphyseal and rami areas) and cancellous bone layers. The total number of elements for all components is 35528: 20236 solid elements (SOLID187: 10-nodes), 15052 contact elements (CONTA174: 8-nodes), and 240 spring elements. In the considered loading case, the mandible is subjected to a bite force and all muscle forces are active and fixed at its extremities (Fig. 6b). The bite force is applied in region A. The applied muscle forces: M^{Right} and M^{Left} denote the sum of masseter muscles (region B and C). T^{Right} and T^{Left} denote Temporalis muscles (region D and E). P^{Right} and P^{Left} denote the sum of medial and lateral pterygoid muscles (regions F and G). The fixation is found in regions H and I. According to the experimental results of Kumar et al. [22], the maximum bite force is assumed to be: $F_b = 44(N)$ after the surgical operation. The muscle forces presented in Table 2 are measured at the maximum capacity of the un-fractured mandible by Mesnard et al. [2], and they are here taken as normally distributed random variables. Following Hasofer and Lind [20], it is preferable to work in a standard normalized space of independent Gaussian variables (Fig. 3b) rather than in the space of physical variables (Fig. 3a). Hence, we adopt the law for a normal distribution, and define a normalized variable u_i by the transformation

$$u_i = \frac{y_i - m_i}{\sigma_i} \tag{11}$$

where y_i is a random variable with its mean value m_i and standard-deviation σ_i. The standard-deviations are assumed proportional to the mean values [21].

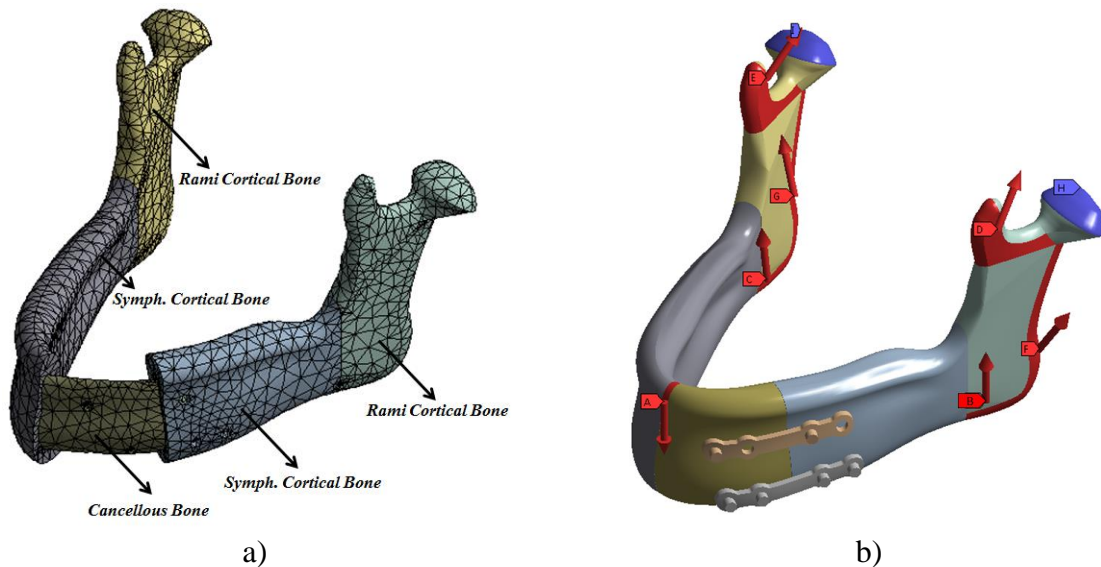
a)   b)

Fig. 6. *a) Meshing model and b) Boundary conditions.*

The random variable vector contains 19 components: 1 for the bite force and 18 for the muscle forces. In order to get sufficient rigidity and a limited displacement at the fracture line, double I mini-plates were fixed to the bone with 6 screws as shown in Fig 6.
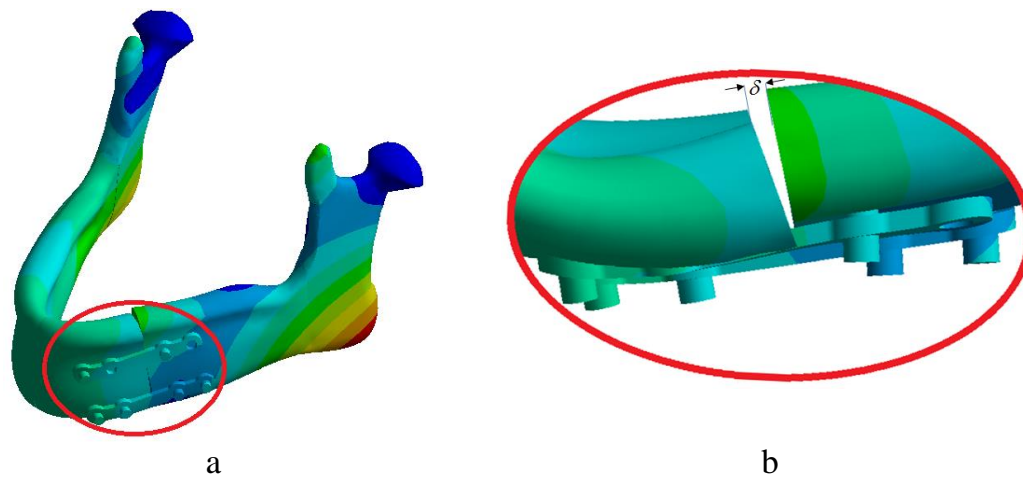
Fig. 7. *a) Total deformation distribution for convalescence period, and b) Normal gap distance between contact and target surfaces.*

The different failure modes are constrained by three conditions: The first condition is that the von Mises stresses of one or several components should not exceed allowable values (Table 1). The second condition is that the contact pressure should not exceed a maximum pressure pain threshold. According to Jensen et al. [23], fifteen patients with 24 mandibular condylar fractures were retrospectively examined with an average follow-up of 23 months. The worst value of the maximum pressure pain threshold was 71 kPa. The last condition is that the relative displacement (gap) between two fracture surfaces should not exceed a prescribed value in order to obtain rapid bone healing. According to the clinical observations of Cox et al. [24], the upper limit of relative movement of the blocks of a broken mandible in the fracture section under a bite force should not exceed 150 μ m which is defined as the limit value of sliding.

3.2. Reliability assessment

After surgical operation, the patient is advised to eat soft foods which render in low bite forces. The muscle forces are automatically produced to balance the mandible system. Here, it is important to introduce the uncertainty of different forces in order to guarantee a safe performance taking into account the osseointegration progress and the overloading possibility. The resulting maximum stress values at the mean point are presented in Table 4. The muscle forces are proportionally calculated relative to the maximum un-fractured mandible capacity [2]. A direct simulation shows that the maximum total displacement is 0.1mm and the maximum von Mises stress occurred in lower mini-plate is 64.45MPa. Here, the maximum initial relative displacement between two fracture surfaces is: $\delta_{\max} = 132(\mu m)$ (Fig. 7a).

When considering the interval variability to be $\pm 50\%$ of the muscle force mean values, both gap and contact pressure constraints are violated. On the basis of Equation (10), the reliability index problem for a double failure mode case can be written as follows:

$$\min : d(u_i) = \sqrt{\sum_{i=1}^{n} u_i^2}$$

$$s.t. \ : H_1(u_i, y_i) = \mathrm{Pr}_{\max}^{Contact}(u_i, y_i) - \mathrm{Pr}_{Threshold} = 0$$

$$: H_2(u_i, y_i) = \delta_{\max}(u_i, y_i) - \delta_w = 0$$

$$: g_1(u_i, y_i) = \sigma_{\max}^{Upper}(u_i, y_i) - \sigma_y^{Metal} \leq 0 \qquad (12)$$

$$: g_2(u_i, y_i) = \sigma_{\max}^{Lower}(u_i, y_i) - \sigma_y^{Metal} \leq 0$$

$$: g_3(u_i, y_i) = \sigma_{\max}^{Right}(u_i, y_i) - \sigma_y^{Bone} \leq 0$$

$$: g_4(u_i, y_i) = \sigma_{\max}^{Left}(u_i, y_i) - \sigma_y^{Bone} \leq 0$$

The first violated constraint is the maximum contact pressure at the fracture line $H(u_i) = \mathrm{Pr}_{\max} - \mathrm{Pr}_{Threshold} = 0$. The resulting reliability index of the studied structure equals to: $\beta = 4.17$ that corresponds to probability of failure $P_f \approx 1.5 \times 10^{-5}$. However, for multiple failure modes, the MPP is located at the intersection point of the maximum gap and contact pressure constraints ($H_1(u_i) = \mathrm{Pr}_{\max} - \mathrm{Pr}_{Threshold} = 0$ and $H_2(u_i) = \delta_{\max} - \delta_w = 0$). This way the maximum pressure should not exceed the threshold value and the maximum gap (relative displacement) at the fracture line should not exceed its allowable limit. Here, the resulting reliability index of the studied structure equals to: $\beta_m = 4.41$ that corresponds to probability of failure $P_f \approx 5.2 \times 10^{-6}$ using equation (8).

4. Discussions

The primary goal of fracture management is healing of the fractured bone resulting in restoration of form and function. Modern traumatology started with the development of osteosynthesis using mini-plates for the treatment of fractures. The correct position of mini-plates is confirmed in the symphysis or parasymphysis fracture respecting the ideal line for osteosynthesis presented by Champy [25]. In our previous work [14], structural optimization strategy has been integrated in order to confirm the surgeon choice for the current clinical case. The topology optimization process is considered as a conceptual design stage to sketch the layout 'or input' to shape optimization. Both shape and sizing optimization are next considered as a detailed design stage. This integrated structural optimization strategy demonstrates the importance of fixation of symphysis or parasymphysis fracture by 2 I plates with 4 holes. In fact, when increasing the number of screws or holes, the biomechanical effects for stabilizing the tow fragments are marginal. The reduction of the number of screws used in the upper plates maintains the stability without any effects for increasing the tension in the region of fracture. This result helps the surgeon to give him the opportunity to reduce the number of screws without any consequence on the stability of fracture with the target to protect adjacent vital structure. However, the previous applied deterministic structural optimization strategy does not take into account the overloading possibility and the muscle forces capacity. Therefore, it is very important to evaluate the reliability level.

In addition, it has been demonstrated that the resulting maximum stress when ignoring the muscle forces, exceeds the yield strength of the bone [14]. However, the integration of different muscle force leads to reasonable values because the muscle forces play a positive role in the equilibrium. According to Table 3, at the MPPs, the resulting bite force values for single and multiple failure modes are almost close to the initial value, that demonstrates the positive role of the muscle forces. During the surgery operation, some muscles can be cut or harmed and it cannot be expected that all muscles will operate at its maximum capacity. Therefore, there is a strong need to introduce the uncertainty on the muscle forces. After having performed a direct simulation where there is no osseointegration layer between fracture surfaces, several failure modes may occur in cases. The first failure case is the contact pressure constraints which should not exceed a maximum pressure pain threshold. The second one is the relative displacement (gap) between two fracture surfaces which should not exceed a prescribed value

in order to obtain rapid bone healing. The last failure mode is the von Mises stresses of different components which should not exceed target values. Here, an equivalent isotropic approximation is integrated to our optimized bone formulation to evaluate the yield stresses of different bone layers when considering orthotropic material behaviors.

The developed algorithm seeks to find the closest point to the limit state verifying a smallest distance to the origin of the normalized space (Fig. 4b). The first violated constraint is the contact pressure. Thus, for a single failure mode, the maximum resulting contact pressure value is: $\text{Pr}_{Threshold} = 59.55 \leq 71 kPa$. However, for multiple failure modes, both gap and contact pressure constraints are violated. The maximum resulting contact pressure value is: $\text{Pr}_{Threshold} = 0.45 \leq 71 kPa$ and the maximum gap value is: $\delta_{\max} = 148 \leq 150 \mu m$ that leads to a larger reliability index value. Therefore, the failure will occur on the pressure constraint violation.

In general, the failure probability of structural studies should be: $P_f \in [10^{-3} - 10^{-5}]$ that corresponds to a reliability index $\beta \in [3 - 4.25]$ however in nuclear and spatial ones, the failure probability should be very small: $P_f \in [10^{-6} - 10^{-8}]$ that corresponds to a reliability index $\beta \in [4.75 - 5.6]$. The different results in Table 4 show a single failure mode with a reasonable value of reliability index $\beta = 4.17$ that corresponds to failure probability $P_f \approx 1.5 \times 10^{-5}$. Thus, the current study leads to reasonable reliability levels when comparing to the structural studies.

4. Conclusions

An efficient reliability algorithm is elaborated to identify the failure modes of the mini-plate fixation strategy used in human mandible fractures. The reliability evaluation is carried out for the period following the surgery operation where there is no connection between the two fracture surfaces. Several scenarios may lead to failure. The first important failure scenario is the von Mises stress of one or several components that represents the fracture indicators. The bone structure possesses anisotropic behaviors. An optimized yield stress/elasticity modulus formulation is integrated using an equivalent isotropic approximation in order to reduce the computing time. The second failure scenario is the contact pressure which should not exceed a maximum pressure pain threshold. The last failure mode is the relative displacement (gap) between two fracture surfaces which should not exceed a prescribed value in order to obtain rapid bone healing. The different results are carried out considering a clinical case of a male patient of 28 years of age. Two critical failure modes are observed: For a single failure mode, the MPP is found on the contact pressure constraint however, for multiple failure modes, the MPP is found on the intersection between the relative displacement and the contact pressure constraints. For future developments of this strategy, it would be possible to find the optimum position of the mini-plates and screws in order to control a required reliability (confidence) level.

Conflict of Interests

The author declares that there is no conflict of interest.

Compliance with Ethical Standards

The patient treatment was done before this research. The research is carried out to evaluate the reliability of the used mini-plates fixation.

References

1. Korkmaz HH. Evaluation of different mini-plates in fixation of fractured human mandible with the finite element method, Oral Surg Oral Med Oral Pathol Oral Radiol Endod 2007;103:e1-e13.

2. Mesnard M, Ramos A, Ballu A, Morlier J, Cid M, Simoes JA. Biomechanical analysis comparing natural and alloplastic temporomandibular joint replacement using a finite element model, J. Oral Maxil. Surg., (2011), 69(4), 1008-1017.

3. Ramos A, Marques H, Mesnard M. The effect of mechanical properties of bone in the mandible, a numerical case study, Advances in Biomechanics and Applications, Vol. 1, No. 1 (2014) 067-076

4. Natali AN, Hart RT, Pavan PG, Knets I. Mechanics of bone tissue. In: Natali AN, editor. Dental Biomechanics. London: Taylor & Francis; 2003. p. 1–19.

5. Robinson RA, Elliot SR. The water content of bone. I. The mass of water, inorganic crystals, organic matrix, and ''CO_2 space'' components in a unit volume of dog bone. J Bone Joint Surg 1957;39A:167–88.

6. Gong, J. K., Arnold, J. S., and Cohn, S. H. (1964), Composition of trabecular and cortical bone, Anat. Rec. 149:325–332.

7. Martin RB. Porosity and specific surface of bone. CRC Critical Reviews in Biomedical Engineering, 1984.

8. Weiner S, Wagner HD. The material bone: structure-mechanical function relations. Ann Rev Mater Sci 1998;28:271–98.

9. Lucchinetti E. Composite models of bone properties. In: Bone mechanics handbook, 2nd ed. Boca Raton, FL: CRC Press; 2001.p. 12.1–19 [chapter 3].

10. Kharmanda G. Reliability analysis for cementless hip prosthesis using a new optimized formulation of yield stress against elasticity modulus relationship, Materials and Design (January 2015), 65: 496-504.

11. Doblare M., Garcıa J.M. and Gomez M.J., Modelling bone tissue fracture and healing: A review, Engineering Fracture Mechanics,71:1809–1840, (2004).

12. Ditlevsen O, Madsen HO. Structural reliability methods, Internet edition, Version 2.2.2; 2005.

13. Haldar A, Mahadevan S. Reliability assessment using stochastic finite element analysis. New York: John Wiley & Sons; 2000

14. Kharmanda G, Kharma A, El-Hami A. Integration of reliability concept into orthodontic prosthesis design: Application on mini-plate fixation systems used in fractured mandibles, Uncertainties and Reliability of Multiphysical Systems, 1 (1), 2017

15. Bonnet AS, Postaire M, Lipinski P. Biomechanical study of mandible bone supporting a four-implant retained bridge: Finite element analysis of the influence of bone anisotropy and foodstuff position, Medical Engineering & Physics 31 (2009) 806–815.

16. Katz JL, Meunier A. The elastic anisotropy of bone. J Biomech 1987;20:1063–70.

17. Akca K, Iplikcioglu H. Finite element stress analysis of the effect of short implant usage in place of cantilever extensions in mandibular posterior edentulism. J Oral Rehabil 2002;29:350–6.

18. Castano MC, Zapata U, Pedroza A, Jaramillo JD, Roldan S. Creation of a three dimensional model of the mandible and the TMJ in vivo by means of the finite element method. Int J Comput Dent 2002;5:87–99.

19. Keaveny TM, Morgan EF, Yeh OC. Bone Mechanics, In: Standard Handbook of Biomechanical Engineering and Design, Chapter 8, (ed. M. Kutz):, 2003 The McGraw-Hill Companies, Inc., ISBN: 9780071356374.

20. Hasofer A.M., Lind N.C. An exact and invariant first order reliability format. J. Eng. Mech, ASCE, EM1, 100, 111-121, 1974.

21. Kharmanda, G. ; El-Hami, A. ; Souza de Cursi (2010): Reliability-Based Design Optimization, In edited book Multidisciplinary Design Optimization in Computational Mechanics, Edited by Piotr Breitkopt and Rajan Filomeno Coelho, Chapter 11, : Wiley & Sons, April 2010, ISBN: 9781848211384, Hardback 576 pp.

22. Kumar ST, Saraf S, Devi SP, Evaluation of Bite Force After Open Reduction and Internal Fixation Using Microplates, Journal of Dentistry, Tehran University of Medical Sciences September 2013; Vol. 10, No. 5

23. Jensen T, Jensen J, Nørholt S.E, Dahl M, Lenk-Hansen L, Svensson P, Open Reduction and Rigid Internal Fixation of Mandibular Condylar Fractures by an Intraoral Approach: A Long-Term Follow-Up Study of 15 Patients, J Oral Maxillofac Surg 64:1771-1779, 2006

24. Cox T, Kohn MW, Impelluso T. Computerized analysis of resorbable polymer plates and screws for the rigid fixation of mandibular angle fractures. J Oral Maxillofac Surg 2003; 61:481-7.

25. Champy M, Lodde JP, Schmitt R, Jaeger JM, Muster D. Mandibular osteosynthesis by miniature screwed plates via a buccal approach. J Maxillofac Surg. 1978; 6 :14-21.

	Cancellous	Cortical Symphyseal	Cortical Rami
E_x **(MPa)**	960	22900	17000
E_y **(MPa)**	390	14200	13800
E_z **(MPa)**	320	10500	10600
ν_{xy}	0.3	0.19	0.38
ν_{yz}	0.3	0.31	0.23
ν_{xz}	0.3	0.29	0.47
G_{xy} **(MPa)**	170	6000	6200
G_{yz} **(MPa)**	130	3700	4100
G_{xz} **(MPa)**	90	4800	5400
K **(MPa)**	371.43	10184.02	13915.15
G **(MPa)**	121.5275	4649.22	5081.49
E **(MPa)**	328.73	12105.51	13590.20
ν	0.35	0.30	0.34
σ_C **(MPa)**	4.72	140	156
σ_T **(MPa)**	3.30 - 4.72	70 - 98	78 - 109

Table 1. *Orthotropic bone materials properties and their equivalent isotropic ones*

Muscle Forces	F_x **[N]**	F_y **[N]**	F_z **[N]**
Superficial Masseter (SM)	18.2	303.3	12.1
Deep Masseter (DM)	7.8	128.3	15.6
Anterior Temporalis (AT)	-18.4	104.8	-43.8
Medial Temporalis (MT)	-6.5	36.3	-53.1
Posterior Temporalis (PT)	-3.4	6.8	-37
Medial Pterygoid (MP)	187.4	325.1	-76.5

Table 2. *Muscle forces [2]*

Parameters		Means	MPP	
			S.F.M.	M.F.M.
F^{Bite} **[N]**	F_y^{Bite}	-44	-47.93	-51.53
M^{Right} **[N]**	M_x^{Right}	5.46	4.58	6.49
	M_y^{Right}	90.64	82.51	67.14
	M_z^{Right}	5.82	4.40	5.74
M^{Left} **[N]**	M_x^{Left}	-5.46	-4.24	-7.70
	M_y^{Left}	90.64	95.77	79.68
	M_z^{Left}	5.82	4.92	7.02
T^{Right} **[N]**	T_x^{Right}	-5.94	-6.00	-7.78
	T_y^{Right}	31.06	27.27	29.10
	T_z^{Right}	-28.12	-21.62	-33.78
T^{Left} **[N]**	T_x^{Left}	5.94	5.58	4.55
	T_y^{Left}	31.06	23.23	22.04
	T_z^{Left}	-28.12	-24.99	-22.52
P^{Right} **[N]**	P_x^{Right}	39.35	29.09	49.32
	P_y^{Right}	68.27	63.89	83.31
	P_z^{Right}	-16.07	-20.26	-12.66
P^{Left} **[N]**	P_x^{Left}	-39.35	-29.71	-55.31
	P_y^{Left}	68.27	52.15	50.89
	P_z^{Left}	-16.07	-18.42	-10.41

Table 3. *Resulting parameter values*

Parameters	Means	MPP	
		S.F.M.	M.F.M.
σ_{max}^{Upper} (MPa)	35.94	31.79	46.80
σ_{max}^{Lower} (MPa)	64.45	51.91	93.92
$\sigma_{max}^{RamiRight}$ (MPa)	22.62	16.58	26.18
$\sigma_{max}^{RamiLeft}$ (MPa)	18.36	15.30	24.63
$\sigma_{max}^{SymRightBack}$ (MPa)	12.64	12.69	15.09
$\sigma_{max}^{SymRightFront}$ (MPa)	6.28	7.93	13.37
$\sigma_{max}^{SymLeft}$ (MPa)	4.66	5.16	6.13
$\sigma_{max}^{CanRightBack}$ (MPa)	0.17	0.12	0.21
$\sigma_{max}^{CanRightFront}$ (MPa)	0.24	0.06	0.36
$\sigma_{max}^{CanLeft}$ (MPa)	0.10	0.11	0.12
δ_{max}^{Cor} (μ m)	132	125	**<u>148</u>**
δ_{max}^{Can} (μ m)	116	113	124
Pr_{max}^{Cor} (kPa)	0	**<u>59.55</u>**	**<u>0.46</u>**
Pr_{max}^{Can} (kPa)	0	0	0
β	---	4.17	4.41
P_f	---	1.5×10^{-5}	5.2×10^{-6}

Table 4. *Resulting response values*